Supporting Information

Vibrational Snapshots of Ultrafast C-H Bond Photoactivation inside a Water-soluble Nanocage

Sunandita Paul[1a], Shashi[1], Ankita Das[1b], Dooshaye Moonshiram[2], and Jyotishman Dasgupta[1]*

[1]Department of Chemical Sciences, Tata Institute of Fundamental Research, Mumbai, India

[2]Instituto de Ciencia de Materiales de Madrid Consejo Superior de Investigaciones, Científicas Sor Juana Inésde la Cruz 3, Madrid 28049, Spain

Current Affiliations:

[a]Department of Chemistry, The University of Chicago, Chicago, Illinois 60637, USA; and the James Franck Institute, The University of Chicago, Chicago, Illinois 60637, USA

[b]School of Chemistry, University of Birmingham, Edgbaston, Birmingham B15 2TT, UK

Materials and Correspondence should be addressed to J.D.;

[*]Email: dasgupta@tifr.res.in

Contents:

1. Materials and Methods:

Chemicals Used: 5-(5-methylthiophene-2-yl)-thiophene-carbaldehyde (BTMC) was purchased from Sigma-Aldrich. For synthesizing the nanocage $PdCl_2$, ethylenediamine and $AgNO_3$ was bought from Merck chemicals. The triazine ligand of the cavity was bought from TCI chemicals and used as purchased.

Sample preparation: Solid Cage powder was weighed and dissolved in water by stirring for 25 minutes at 60°C in oil bath to prepare a 2.5 mM solution. Five molar equivalent of solid BTMC powder was weighed and added to the Cage solution, and stirred in dark for 30 minutes in a glass vial at room temperature and ambient pressure. The solution was then syringe filtered to remove the excess solid BTMC in solution. This was used for all further ultrafast experiments. The FSRS experiments were done in 5 mM Cage solution.

Synthesis of the cationic (Pd6L4) Cage: Cage was prepared according to the reported literature by M. Fujita et al. *Nature*, 1995, 378, 469. A solution of $Pd(En)(ONO_2)_2$ in H_2O was taken to which 2,4,6-tri(4- pyridyl)-1,3,5-triazine was added in a molar ratio of 6:4. The suspension then stirred for 24 hrs and then heated at 80 C for 2 hrs. It was then filtered hot and washed with hot water [1-2]. The filtrate was then evaporated to dryness and a pale white powder was obtained. ^{1}H NMR was recorded for characterization (600MHz, D_2O, 298 K): δ 9.00 (d, 24H, pyridine-α), 8.51 (d, 24H, pyridine-β), 2.85 (s, 24H) as shown in Figure S1.

Steady State Optical Spectroscopy: Steady state absorption measurements were carried out in JASCO V-670 spectrophotometer. All absorption measurements were done by appropriately diluting a 2.5 mM stock solution in a quartz cuvette of 1 mm pathlength. We used 250 μM concentration for absorption measurements of the empty Cage in water and the free BTMC solubilized in $CHCl_3$. For the mixture that is the host-guest complex we used 2.5 mM of the complex with 1:1 host-guest stoichiometry.

Steady State Raman Measurements: Steady state Resonance Raman measurements were done on Alpha 300R confocal Raman microscope of WITec GmbH, Ulm (Germany). The resonance excitation was done at 488 nm using a solid state frequency-doubled DPSS Nd:YAG laser. It is a confocal Raman setup where a100 μm optical fiber was used to collect the backscattered photons focused on a lens-based ultrahigh throughput spectrometer (UHTS300) with 1800 grooves/mm grating, which was coupled to a back-illuminated CCD camera (1024 × 128 pixels, Peltier-cooled to −65 °C) for detection. The spectral resolution

achieved was ~2 cm^{-1}. To prevent degradation of sample, it was circulated in a flow quartz flow cuvette of 2 mm thickness on which the excitation laser was focused by a 10x lens.

Femtosecond Transient Absorption Measurements: Time resolved absorption measurements were done using femtosecond transient absorption setup which has been described in details previously[3]. A mode-locked femtosecond (~10 fs) pulse was generated using Ti-Sapphire crystal with bandwidth of ~100 nm and ~400 mW power at a repetition rate of 80 MHz (Coherent Micra-5 Mode-locked Ti:sapphire Laser system). It was then amplified using chirp pulse amplification in a commercial regenerative amplifier (Coherent Legend Elite Ultrafast Amplifier Laser system) to produce ~30 fs pulses at 800 nm (65 nm bandwidth) with 3.5 W power and 1 KHz repetition rate. The output from the amplifier was then doubled by a LBO crystal to get 400 nm excitation pulse. A white light continuum was generated by focusing a small portion of the 800 nm pulse from the amplifier on a 2 mm thick sapphire crystal. This was used as a probe with frequency ranging from 420 nm to 1400 nm . The pump was passed through a one-meter-long motorized translation stage outfitted with a quadra-pass mirror assembly delay stage for setting the time difference between the pump and probe. Both the pump and the probe were focused on the sample stage spatially and temporally. All measurements were carried out in a 1 mm flow cuvette connected to a peristaltic pump to circulate the liquid for avoiding any sample photodegradation. The IRF was ~120 fs for the measurements. The focal spot was ~150 μm is diameter. The pump power used for TA measurements was ~70 nJ/pulse for host-guest complex and ~100 nJ/pulse for BTMC in $CHCl_3$.

Kinetic Data Fitting Procedure: Single wavelength kinetic fits for transient absorption was fitted using multi-exponential decay constants in convolution with the respective instrument response function (IRF). It was done in Igor Pro5 Wavemetrics software to get the lifetime and amplitude of each decay component. The equation used was:

$$y = A_0 + \Sigma A_i e^{(-t/\tau i)}$$

Global Analysis of TA data: Global analysis of the TA data was done using Glotaran 1.5.1 software. Single value decomposition was done to obtain the Evolution associated spectra (EAS) and their corresponding lifetimes[4].

FSRS set up and signal processing: Time resolved Raman measurements were done using femtosecond stimulated Raman spectroscopy setup which has been described in details

previously[5,6]. For the FSRS measurements a ~2.5 ps Raman pump pulse was used along with the actinic pump and probe pulses with IRF ~150 fs. A part of the 800 nm beam from the amplifier was stretched by a pair of grating and slit to generate the picosecond Raman pump pulse. The Raman pump power was kept at 1.5 μJ/pulse with an actinic pump pulse of 150 nJ/pulse. The Raman spectral resolution was ~16 cm^{-1} as measured using the 802 cm^{-1} cyclohexane peak. The probe pulse in the NIR region was compressed by a pair of prism for chirp correction and generation of vibrational coherence. The Raman (~200 μm spot size) and probe (~80 μm spot size) were incident together on the sample after variable time delay of actinic pulse excitation. Stimulated Raman signal is obtained from the sample if both the Raman pump and probe pulses are overlapped temporally and spatially on the sample and we detect log (IRaman+Probe/IProbe). For FSRS experiments, we record two datasets: stimulated Raman spectra (SRS) without and with actinic pump. SRS without actinic pump contain ground state. After solvent peak subtraction and baseline correction, we obtain ground state Raman spectra (GSR). SRS with actinic pump can be processed to obtain excited Raman spectra (ESR) as described below. The subtraction of SRS spectra (SRS with actinic pump on - SRS without actinic pump) give 1) bleach of ground state, 2) signal from excited state and 3) a baseline coming mainly from transient absorption and other nonlinear processes. In this case we found very prominent excited state Raman signatures which compensated for the ground state bleach signal. The baseline was then corrected for the excited state Raman spectra and peak fitted. The area under the peak was integrated to evaluate the dynamics of the modes.

Theoretical studies: The optimized structure and normal mode analysis of ground state of BTMC was done by CAM-B3LYP/6-31g(d). The Raman intensities were calculated and compared with our observed stimulated Raman spectra as shown in Figure S 20. The S1 state of BTMC was then optimized and Raman spectra calculated. The D0 and D1 state for both radical cation and neutral radical was then computed with their Raman intensities using u-CAM-B3LYP/631g(d). Gaussian 16 package was used to run the computations[6]. The geometry optimization was carried out using the default criteria 1.00D-08 in convergence on RMS density matrix and 1.00D-06 in convergence in energy change. For all the optimized geometry both in ground state and excited state normal mode calculations were done and confirmed that there were no imaginary frequencies.

For computing the neutral Cage and its corresponding Cage anion radical spectrum we employed the ORCA (Version 6.0.1) program package developed by Neese[4] and co-workers.. The DFT optimizations were conducted using the HF-3C functional[5] as well as the BP86

exchange-correlation functional[6] in combination with the double zeta valance polarization functions (def2-SVP)[7]. The RI[8] approximation with the auxiliary basis def2/J[9] were used to accelerate Coulomb and exchange integrals for the ground and excited state calculations respectively. The default GRID settings were further used for the self-consistent field iterations and for the final energy evaluation.

The Raman calculations for the Cage complexes were the conducted using the VWN5 functional[10] in combination with STO-3G[11-12] . The calculated structures were confirmed to be minima based on a check of the energies and the absence of imaginary frequencies from frequency calculations carried out on the optimized geometries. The frequency run was further combined with a polarizability calculation to calculate the Raman spectral features.

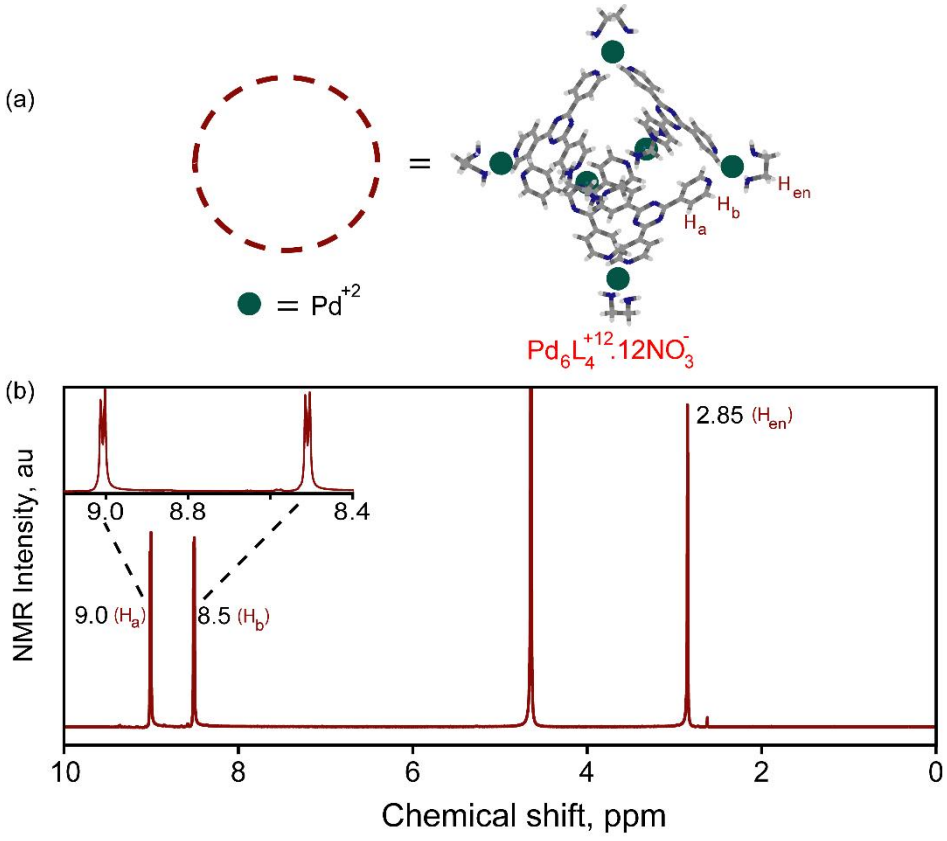

Figure S1. (a) Structure of Cage ($Pd_6L_4^{+12}$) (b) NMR of 2.5 mM Cage solution in D_2O

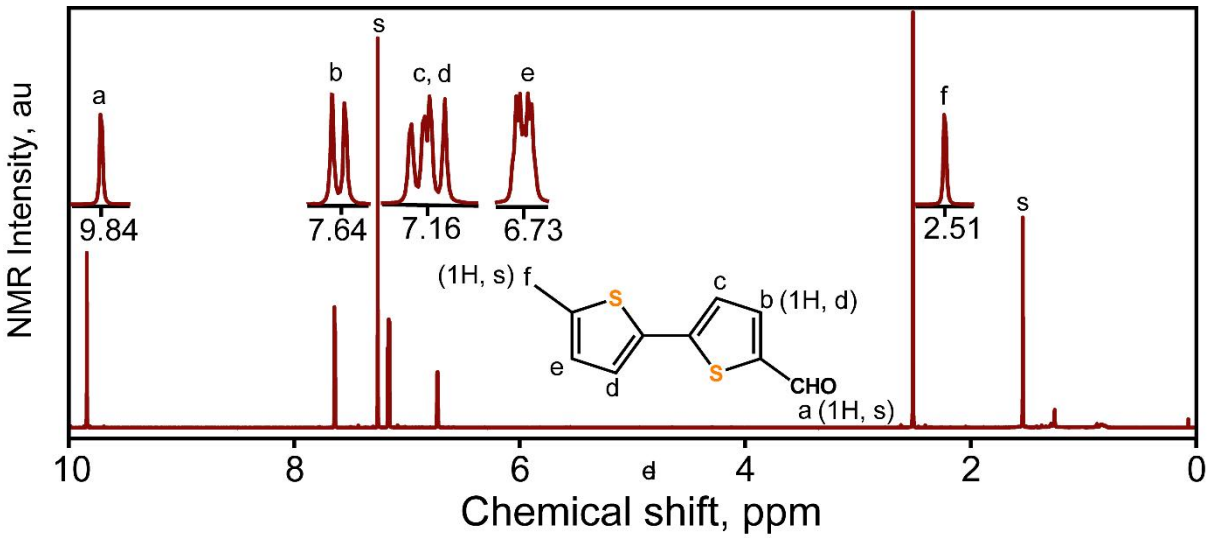

Figure S2. NMR of BTMC solution in $CDCl_3$

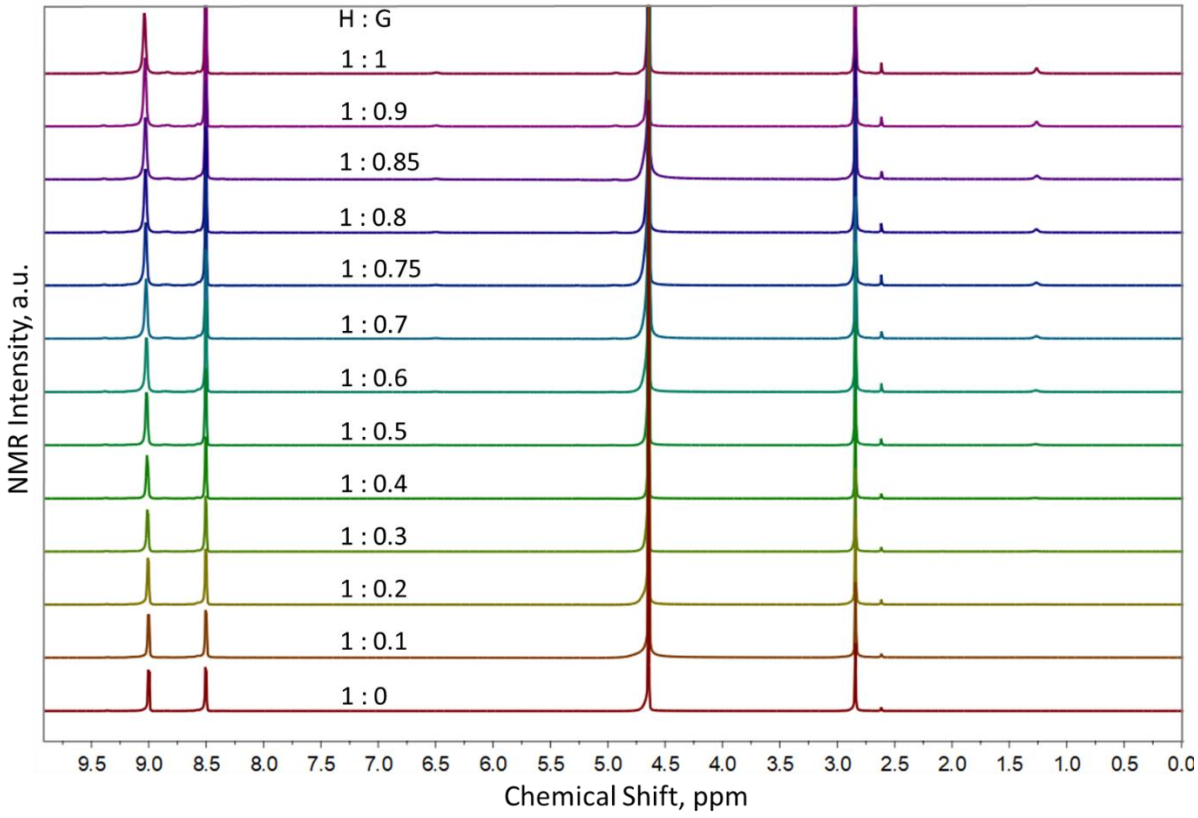

Figure S3. ^1H NMR binding titration of BTMC⊂Cage at different BTMC concentrations starting from 2.5 mM Cage in D_2O (H : G = host and guest relative ratios).

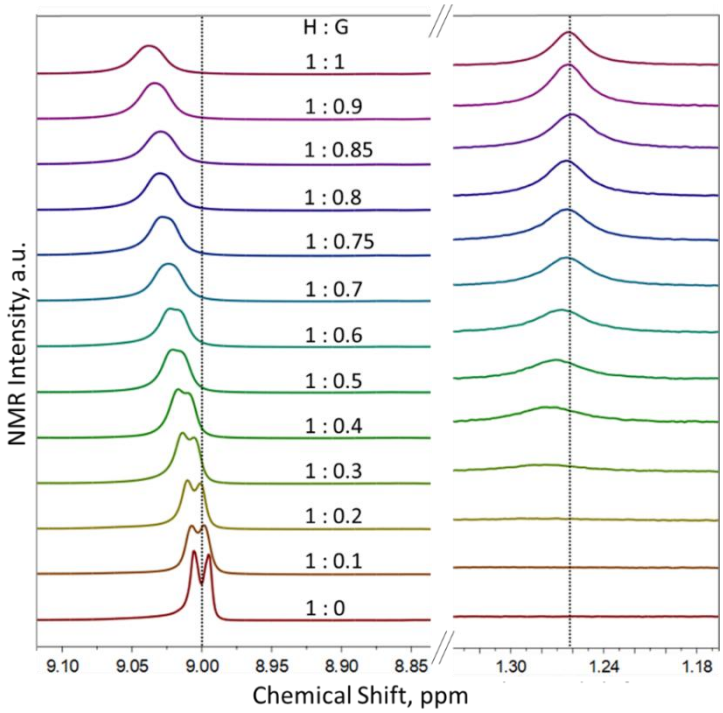

Figure S4. Magnified ^{1}H NMR binding titration of BTMC⊂Cage at different BTMC concentrations starting from 2.5 mM Cage in D_2O (H : G = host and guest relative ratios). The spectra shows increasing aliphatic proton from BTMC with saturation at 1:1 complex along with shift and broadening of cavity proton due to host guest complex formation.

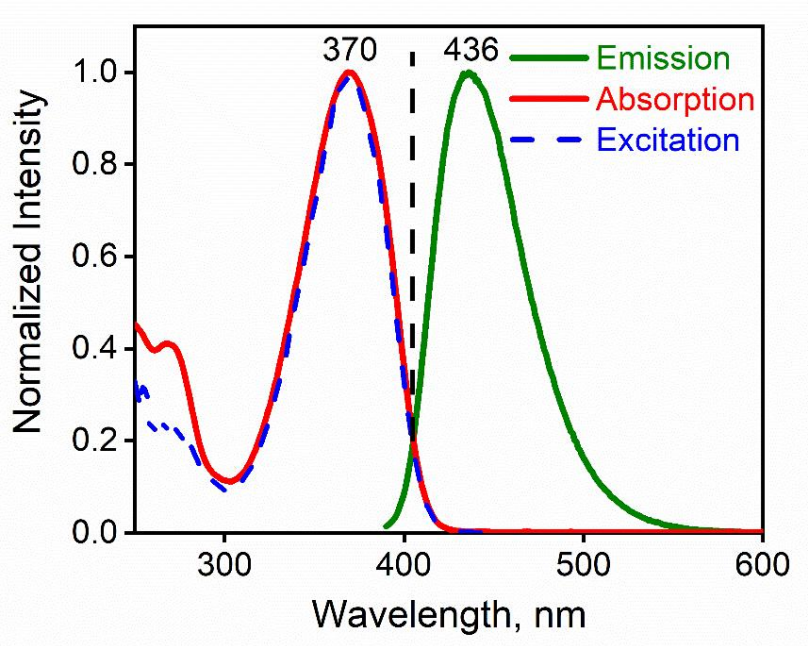

Figure S5. Steady state absorption, emission and excitation spectra of BTMC in $CHCl_3$. The red trace shows steady state absorption, the green trace shows the emission spectra and the blue dotted line shows the excitation spectra.

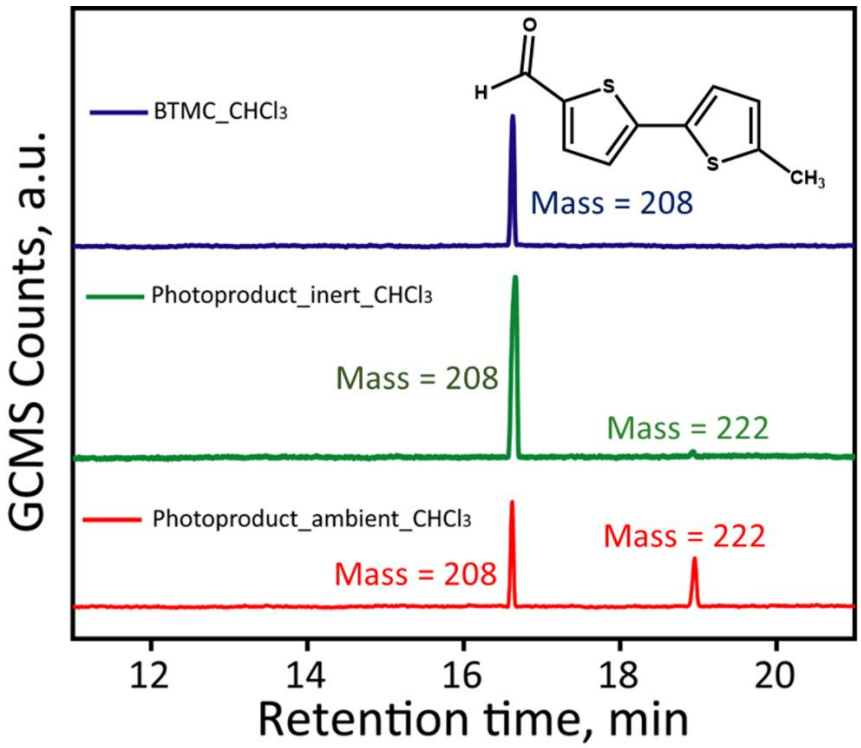

Figure S6. GCMS trace showing pure BTMC (blue trace), product formed after photoreaction of BTMC⊂Cage under inert conditions (green trace) and ambient conditions (red trace) in $CHCl_3$.

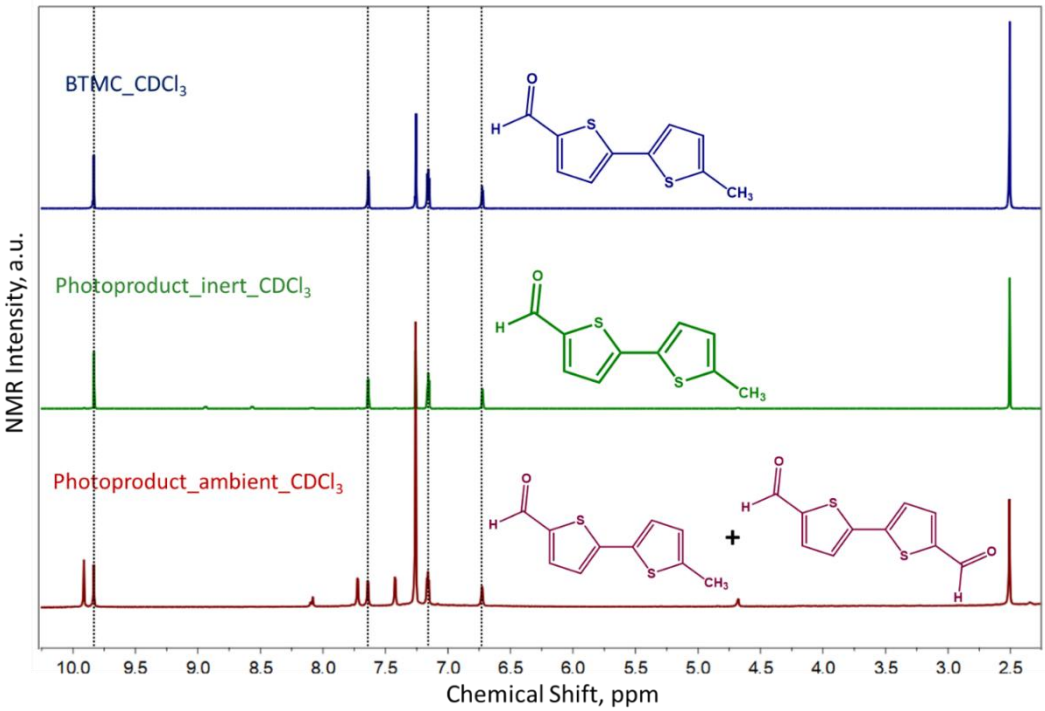

Figure S7. ^1H NMR spectra showing pure BTMC (blue trace), photoproduct of BTMC⊂Cage under inert conditions (green trace) and ambient conditions (red trace) after extraction in $CDCl_3$.

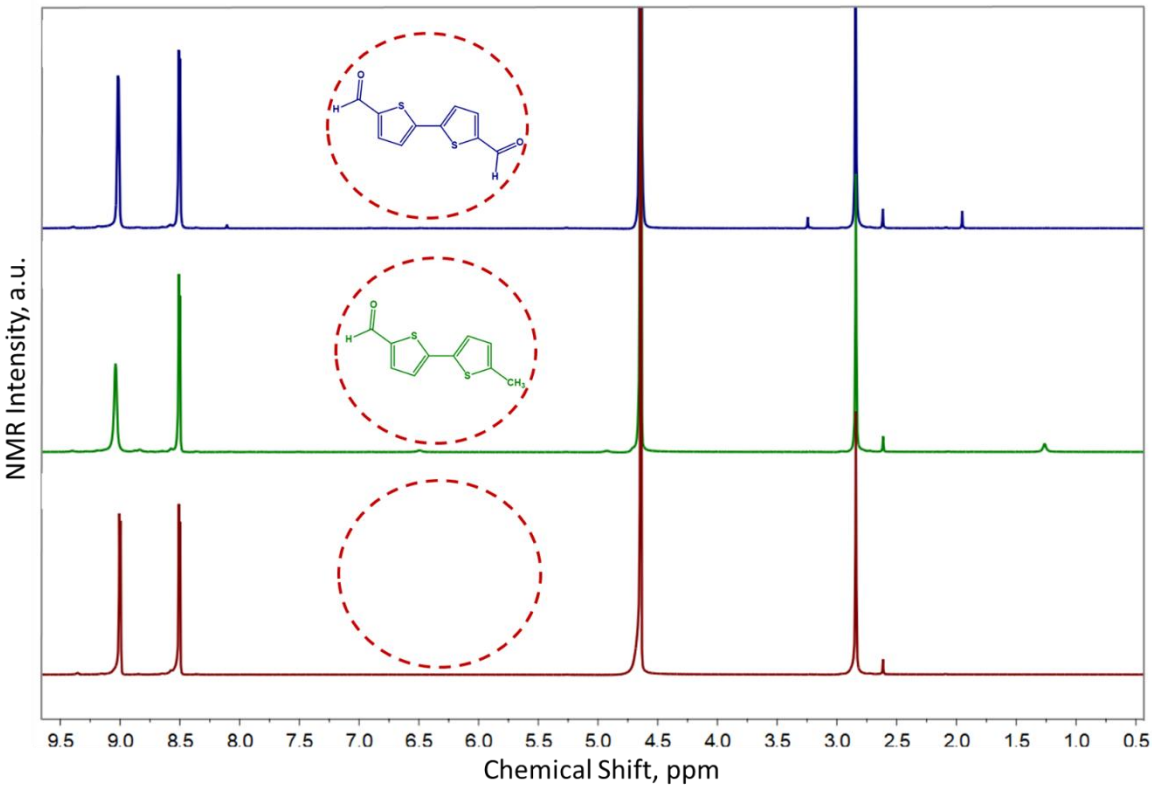

Figure S8. ^{1}H NMR spectra showing Cage (red trace), BTMC⊂Cage (green trace) and photo-product⊂Cage in D_2O (blue trace).

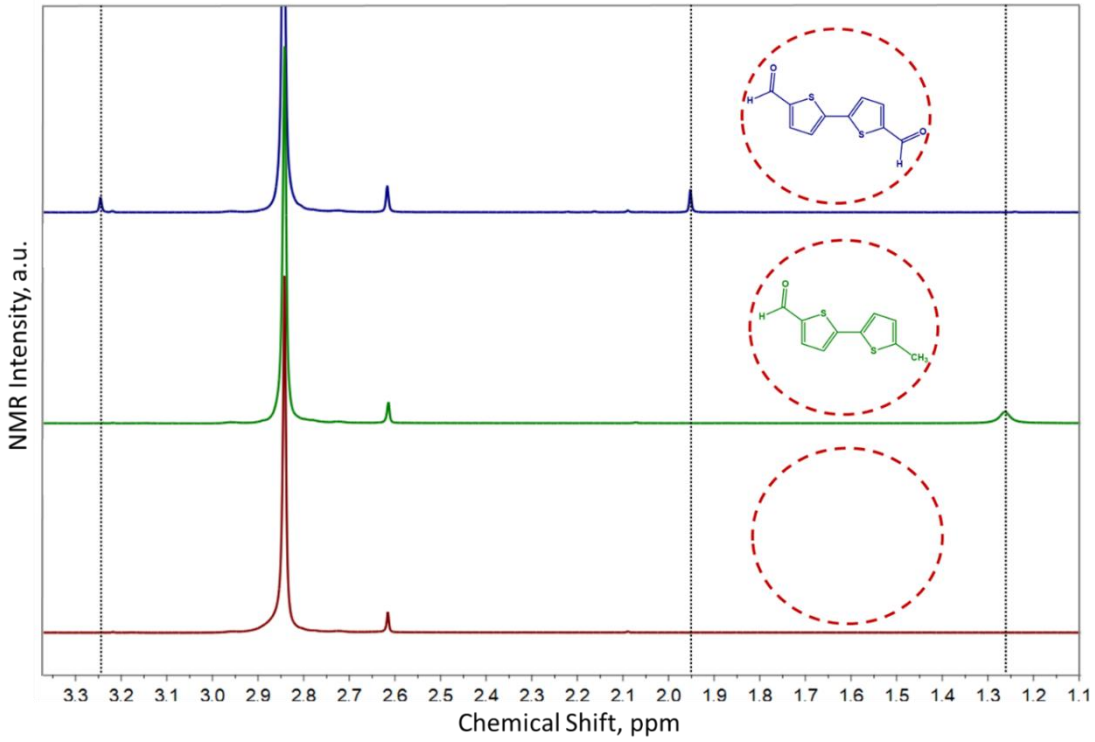

Figure S9. Magnified ^{1}H NMR spectra showing Cage (red trace), BTMC⊂Cage (green trace) and photo-product⊂Cage in D_2O (blue trace).

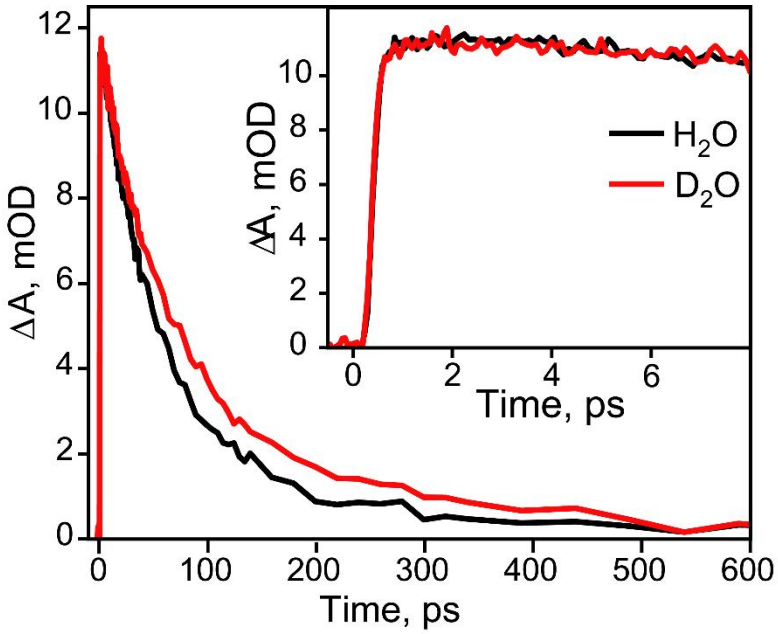

Figure S10. Single point kinetics at 460 nm showing TA decay of BTMC⊂Cage in H_2O (black) and D_2O (red) showing slower decay in D_2O. The initial time points as shown in the inset show similar dynamics in both the solvents.

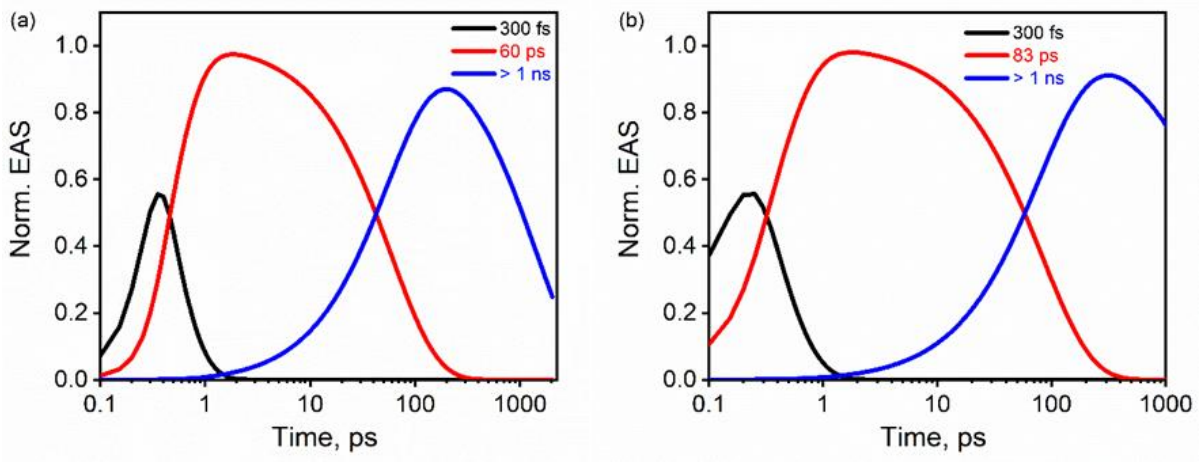

Figure S11. Kinetics from SVD of the TA of BTMC⊂Cage showing a three-state sequential model in (a) H_2O (b) D_2O

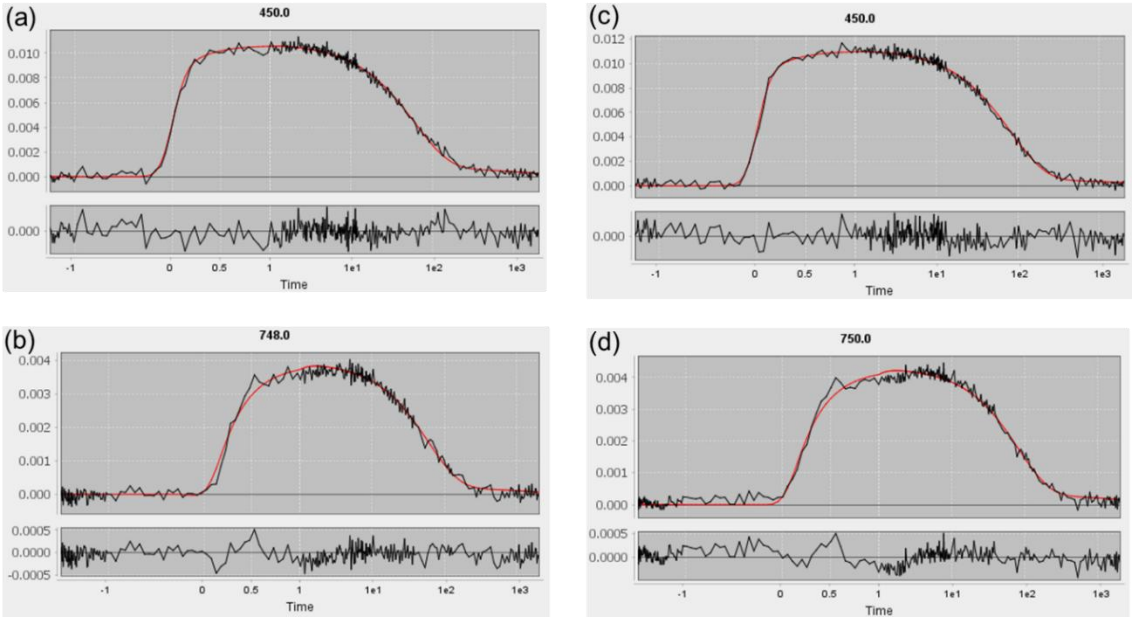

Figure S12. Single point fitting and the corresponding residual traces from transient absorption global analysis of BTMC⊂Cage at a) 450 nm, b) 748 nm in H_2O and c) 450 nm, d) 750 nm in D_2O.

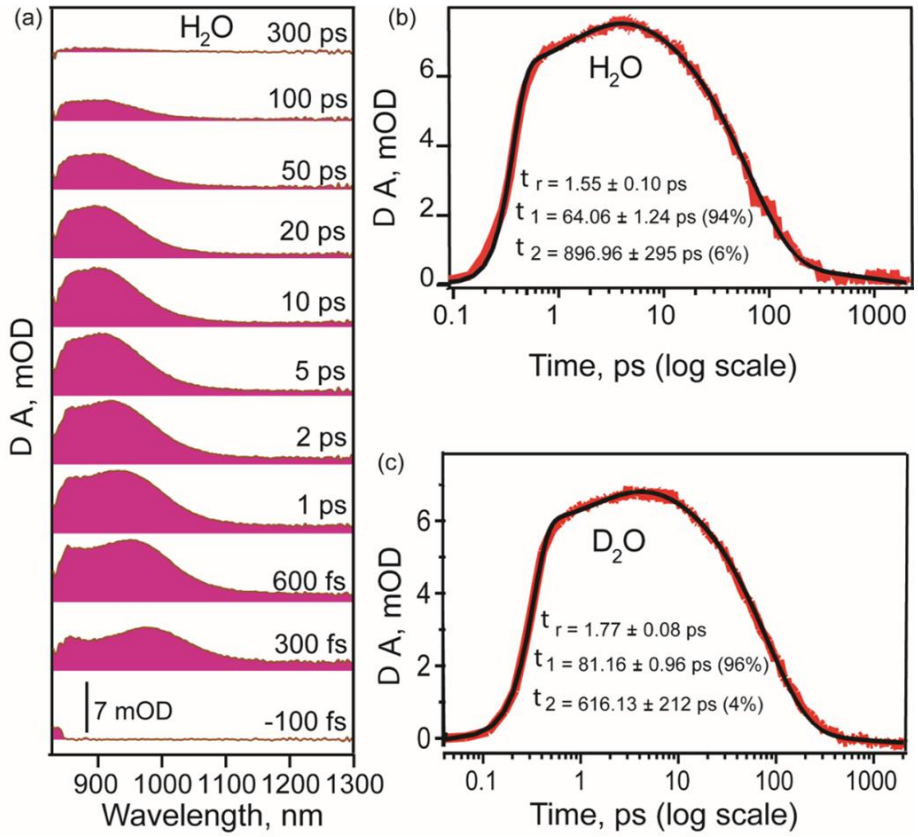

Figure S13. (a) fs-ns transient absorption of BTMC⊂Cage in the probe region of 850-1300 nm on 400 nm excitation (b) Single point Kinetics at 880 nm in H_2O (b) Single point Kinetics at 880 nm in D_2O

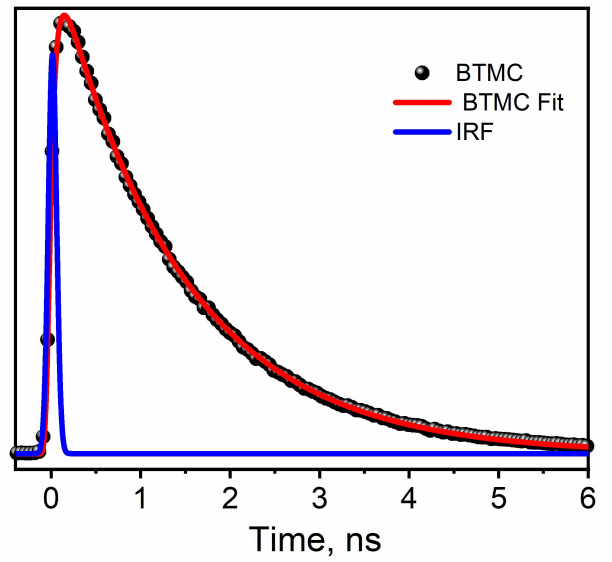

Figure S14. TCSPC measurement of BTMC in $CHCl_3$ after 285 nm excitation and emission lifetime observed at 450 nm. The black dots show the raw data with the fit being shown as red trace. The blue line shows the fitted IRF of the setup which has a 65 ps width. We observe a deconvoluted rise time of 57 ps and mono-exponential decay of 1.39 ns.

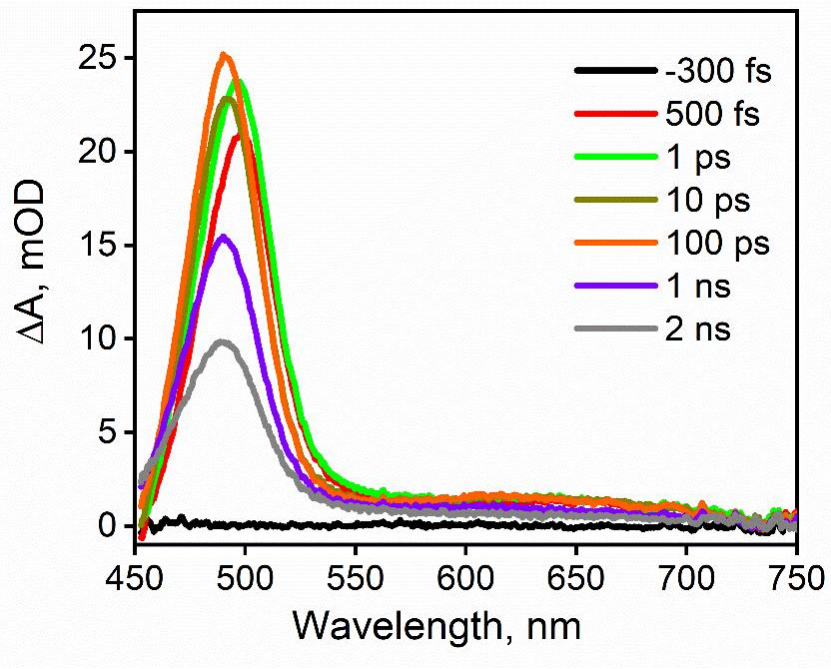

Figure S15. fs-ns transient absorption of BTMC monomer solution in $CHCl_3$ after photo excitation by 400 nm fs pulsed laser.

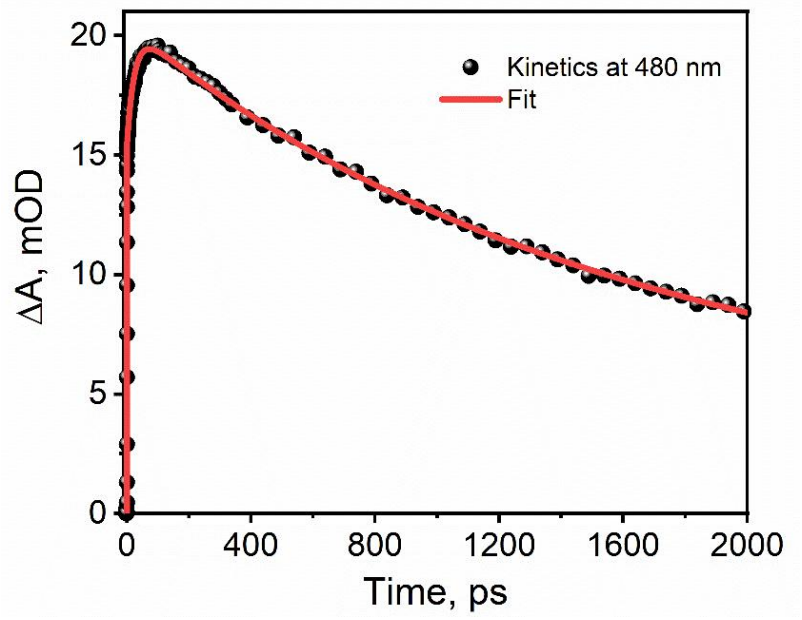

Figure S16. Single point kinetics of fs-ns transient absorption of BTMC monomer solution in $CHCl_3$ at 480 nm. The decay kinetic was fitted with a rise and two exponential decay. We observe a risetime of 24.3 ps and bi-exponential decay of 1.2 (53%) ns and >2 ns (47%).

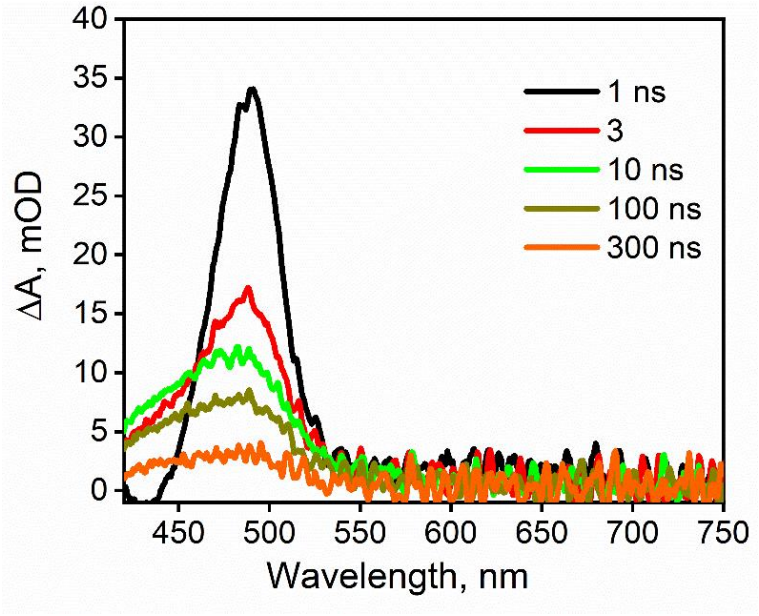

Figure S17. ns-µs transient absorption spectra of BTMC monomer solution in $CHCl_3$ at various delay times after photo excitation by 400 nm fs pulsed laser.

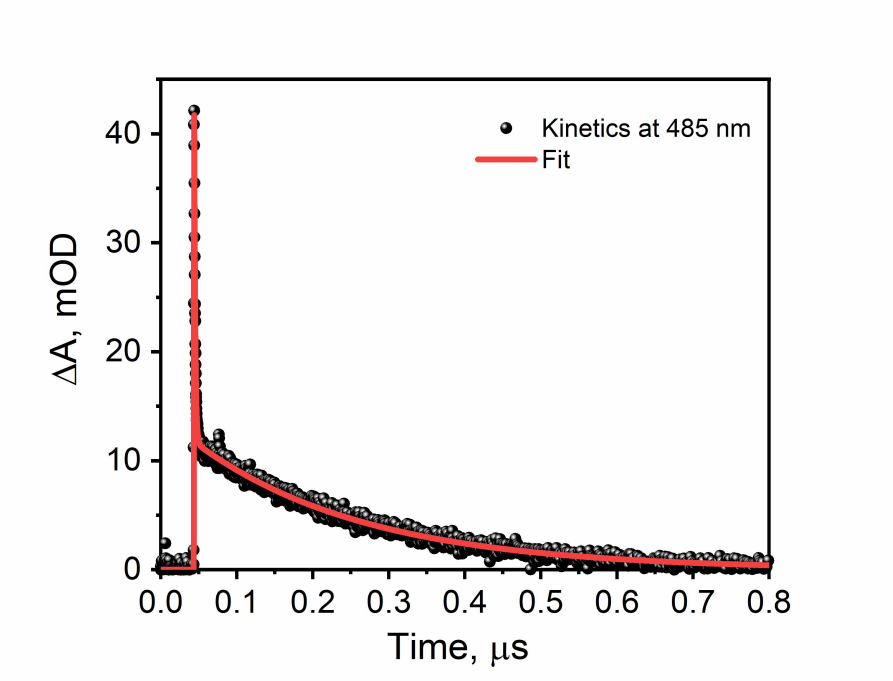

Figure S18. Single point kinetics of ns-μs transient absorption of BTMC monomer solution in $CHCl_3$ at 485 nm. The decay kinetic was fitted with a rise and bi-exponential decay of 1.3 ns and 0.22 μs.

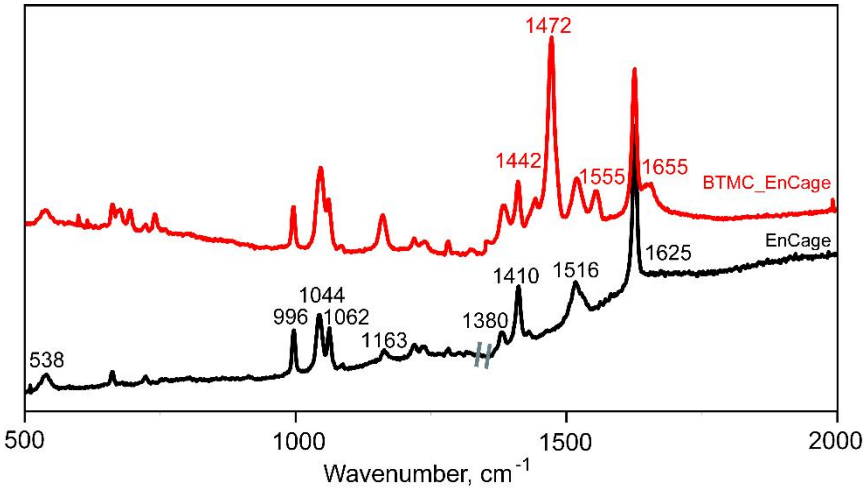

Figure S19. Steady state Raman spectroscopy of BTMC⊂Cage. The black trace shows the Raman spectra for 2.5 mM empty Cage in H_2O. The red trace shows BTMC ⊂ Cage. Molecular modes are marked in red in addition to the cavity modes.

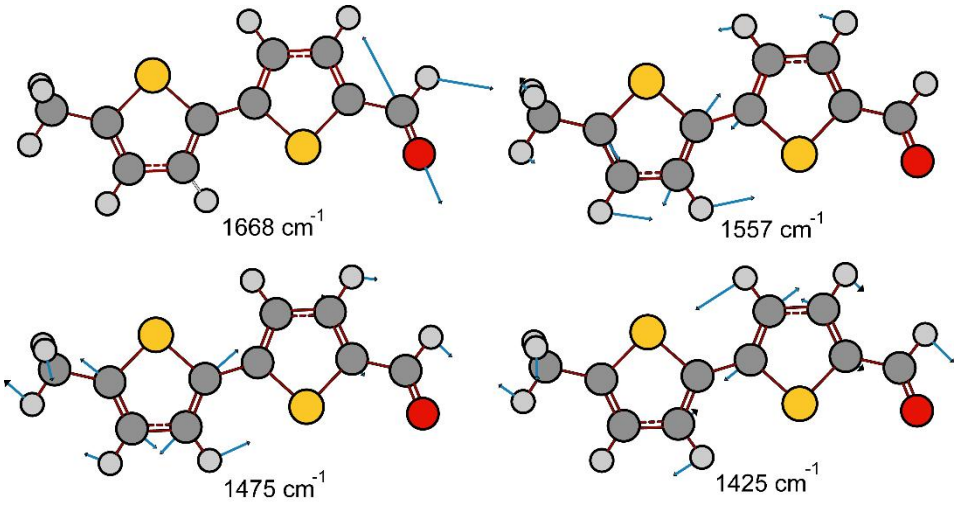

Figure S20. Computed Raman modes of BTMC ground state with CAM-B3LYP/ 6-31G(d)

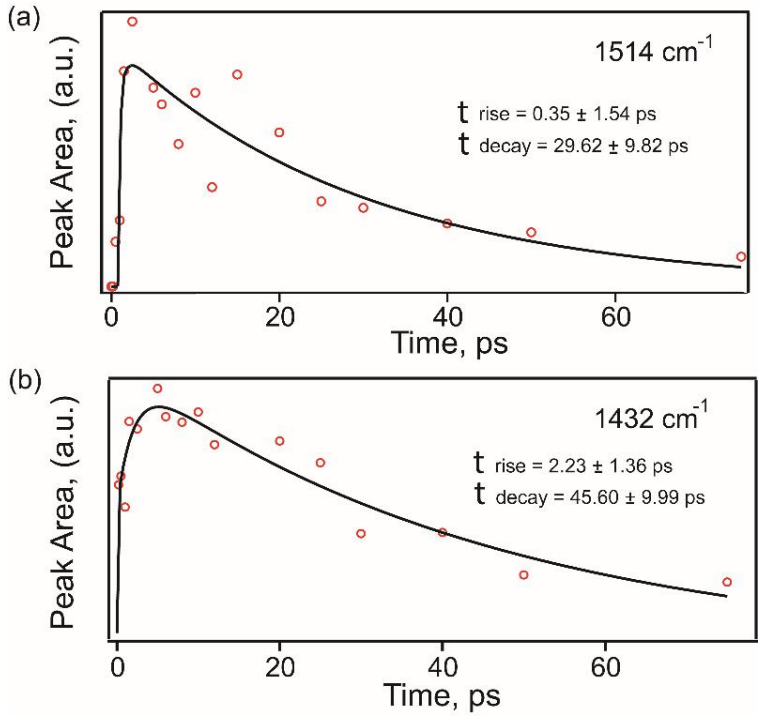

Figure S21: Single mode kinetics of PCET process obtained from the FSRS data by integration of the area under the peak for modes at 1432 cm^{-1} and 1514 cm^{-1}.

(a)

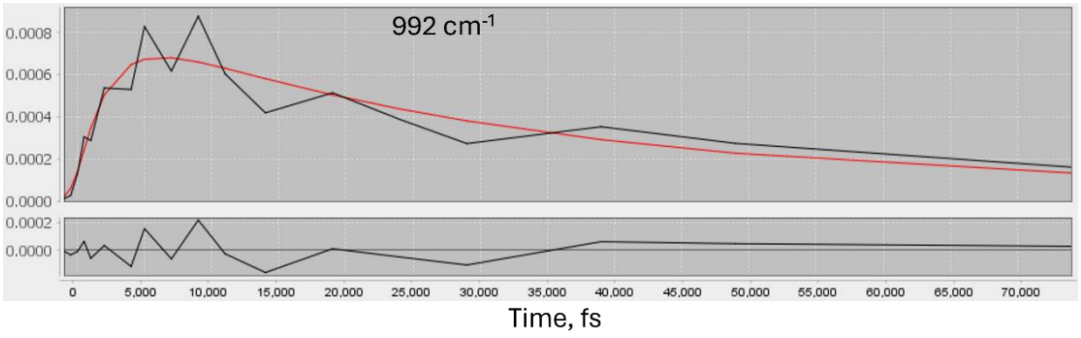

(b)

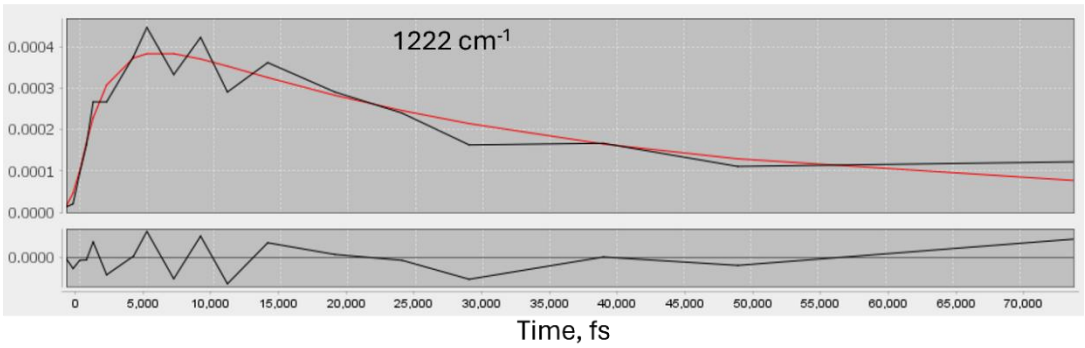

Figure S22: Single point fitting and the corresponding fir residuals from FSRS global analysis at 992 and 1222 cm^{-1} respectively.

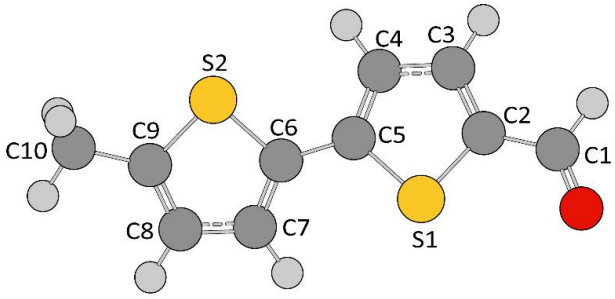

Index	BTMC S_0	BTMC S_1	Rad Cat D_0	Rad Cat D_1	Radical D_0	Radical D_1
C9 - C10 Bond length (BL) in Å	1.49	1.48	1.48	1.49	1.36	1.38
C9 – C8 BL	1. 36	1.38	1.40	1.38	1.42	1.40
C8– C7 BL	1.42	1.39	1.37	1.39	1.38	1.39
C7-C6 BL	1.36	1.41	1.41	1.39	1.39	1.38
C6– C5 BL	1.45	1.38	1.40	1.40	1.42	1.42
C9 - S2 BL	1.73	1.73	1.72	1.71	1.76	1.75
S2-C6-C5-S1 Dihedral in degrees	169.72	179.99	179.87	179. 99	180	179.99

Figure S23. Optimized structure of BTMC in S_0 state is shown. The table depicts the change in the structure in various electronic states showing the change of bond lengths and bond angles.

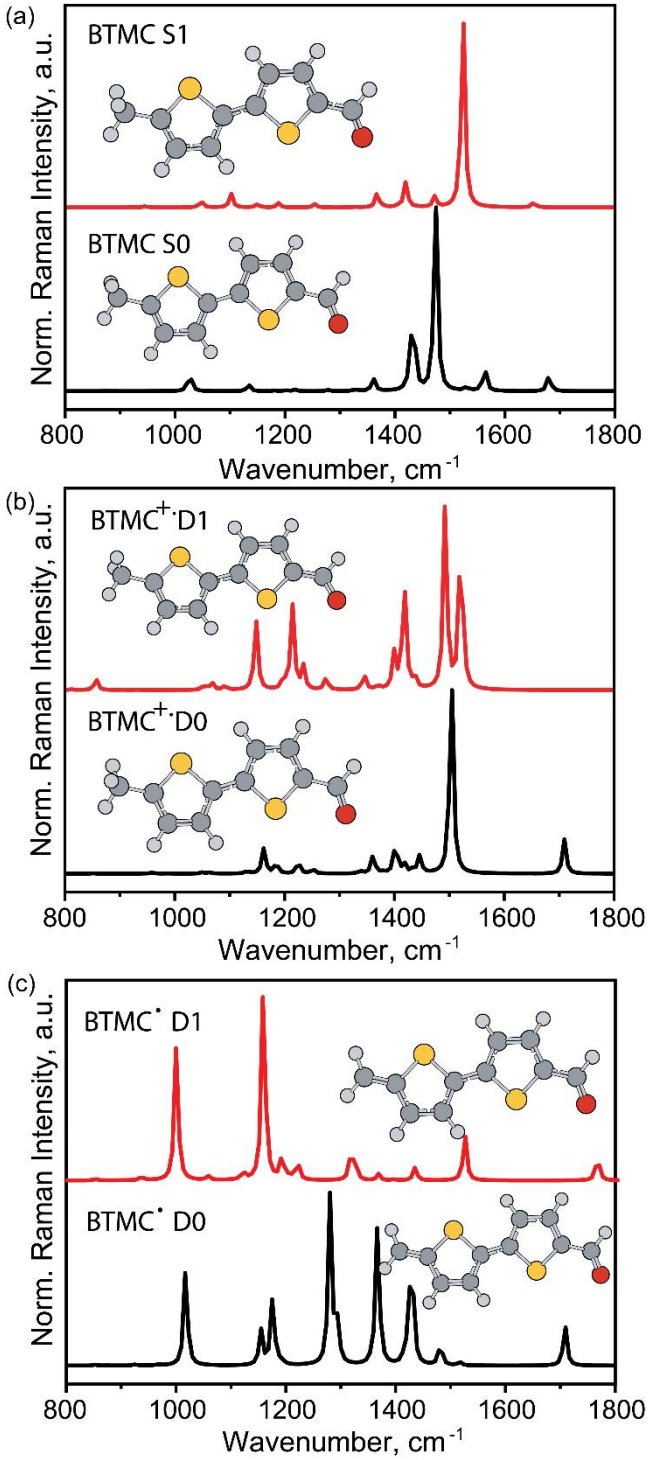

Figure S24. (a) Computed Raman spectra (unscaled) of BTMC in the S_0 state (black trace) and S1 state (red trace) along with the respective optimized structures. (b) Computed Raman spectra of BTMC radical cation (unscaled) in the D0 state (black trace) and D1 state (red trace) along with the respective optimized structures. (c) Computed Raman spectra of BTMC neutral radical (unscaled) in the D0 state (black trace) and D1 state (red trace) along with the respective optimized structures. Our experimental results of FSRS show the match of Raman spectra for D0 state of BTMC radical cation which then evolves to the D1 state of BTMC radical.

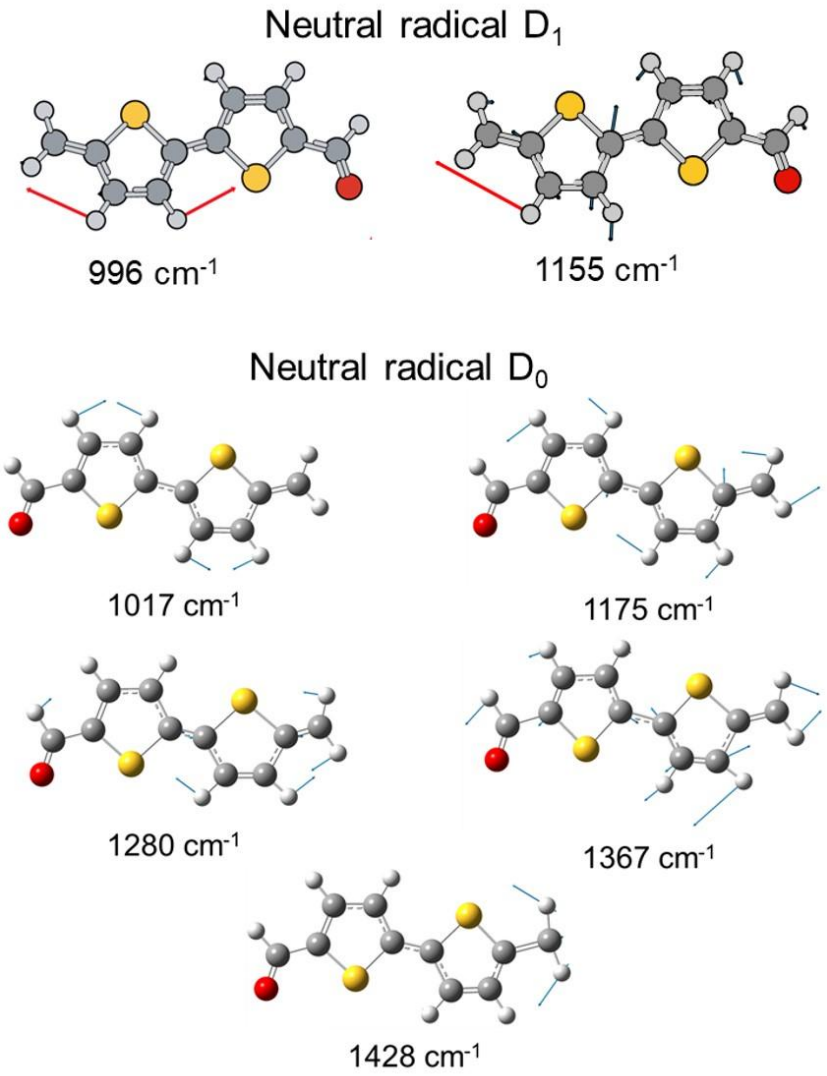

Figure S25. Computed Raman modes of BTMC neutral radical after scaling in D_1 and D_0 state with uCAM-B3LYP/ 6-31G(d).

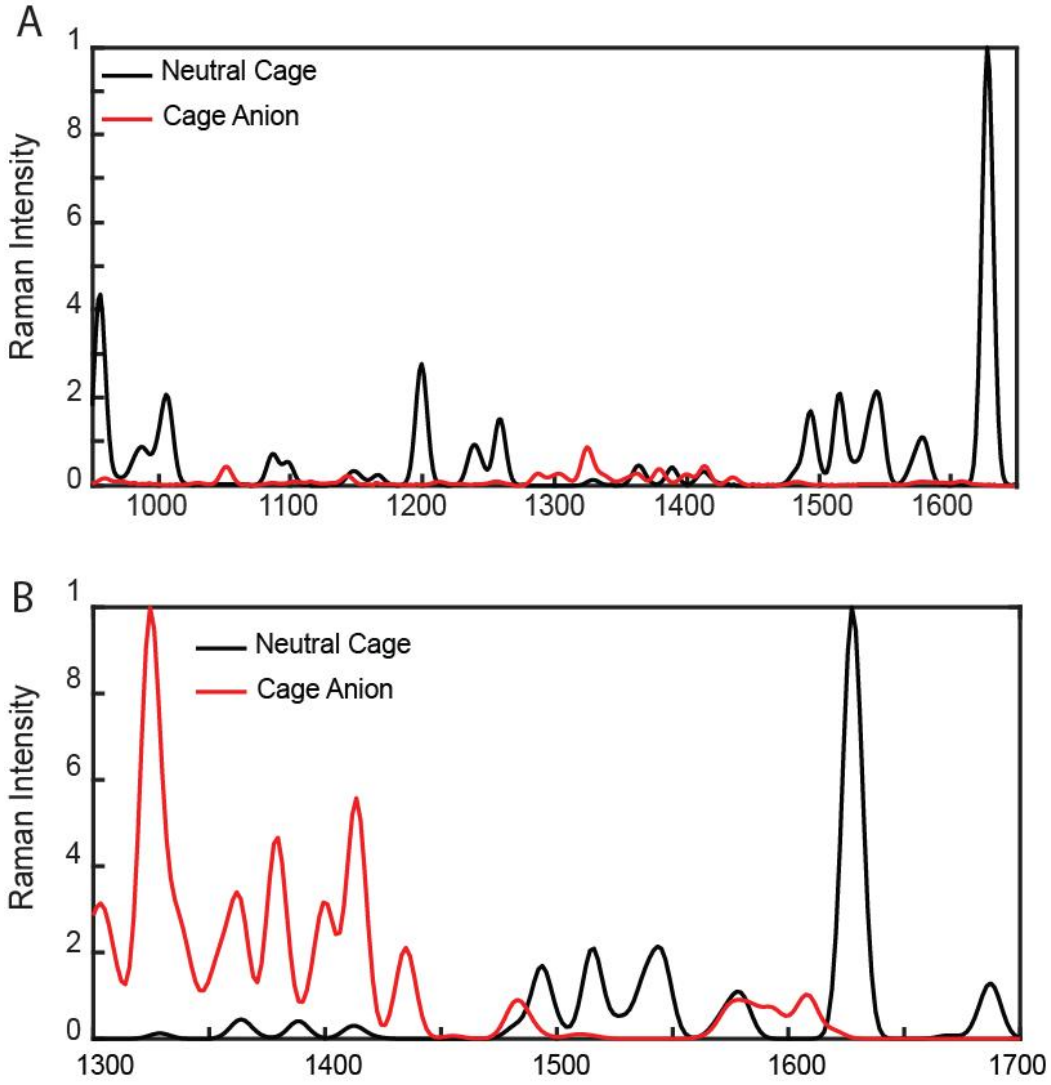

Figure S26. (A) Computed Raman spectra of the neutral Cage and the Cage anion-radical, showing vibrational modes from 950–1700 cm^{-1}. Raman intensities are plotted using the true calculated Raman cross-sections and normalized to the 1625 cm^{-1} peak of the neutral Cage. All vibrational frequencies were uniformly scaled by a factor of 0.96. Computational details are provided in the text. **B)** Comparative Raman features of the neutral Cage and the Cage anion-radical, with the spectra normalized to the strongest peaks at 1625 cm^{-1} (neutral Cage) and ~1330 cm^{-1} (anion-radical). The comparison clearly demonstrates that the Cage anion-radical is expected to exhibit dominant vibrational features in the 1300–1700 cm^{-1} region.

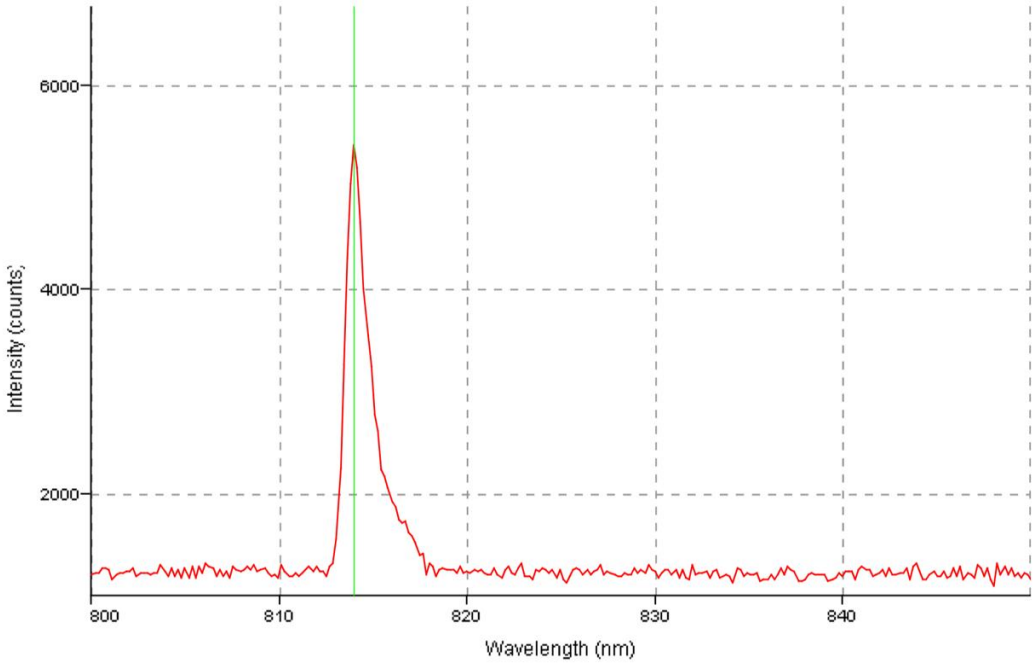

Figure S27. Raman pump spectra for FSRS measurements centered at 814 nm.

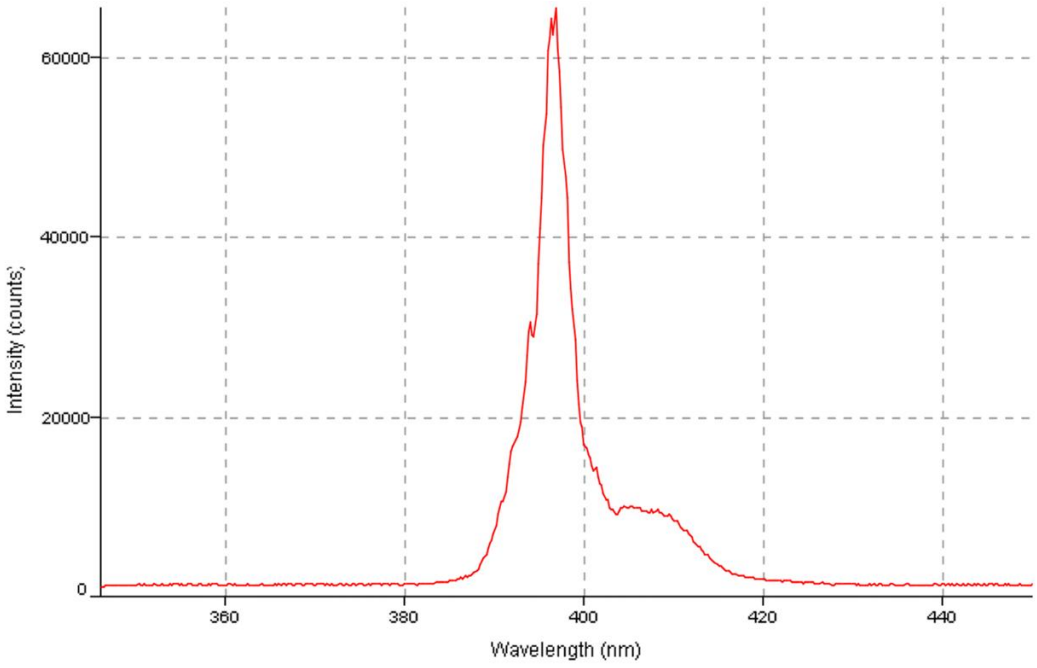

Figure S28. Actinic pump spectra for FSRS measurements centered at 395 nm.

Table 1

Coordinate for optimized S0 of BTMC

C	-3.47338800	-0.23312300	0.01530700
C	-2.89057300	-1.45875800	-0.11989000
C	-1.47012300	-1.41248400	-0.15798000
C	-0.96633300	-0.14451400	-0.05024300
S	-2.26487500	1.01168400	0.10355400
C	0.41969100	0.28174700	-0.05211600
C	0.91194300	1.56574500	-0.13349100
C	2.32221700	1.61821200	-0.11088400
C	2.90248200	0.37885700	-0.01323000
S	1.70705100	-0.87922200	0.06163200
C	-4.93012000	0.09773300	0.08804700
C	4.31631400	0.06832900	0.03101300
O	4.77078600	-1.06042600	0.11602400
H	-3.46427300	-2.37538300	-0.19408100
H	-0.84658600	-2.29231300	-0.27122700
H	0.27854300	2.44075300	-0.21721400
H	2.89720300	2.53541400	-0.16955500
H	-5.51798000	-0.82104300	0.02788500
H	-5.18421900	0.60312500	1.02508300
H	-5.23787100	0.75245200	-0.73337200
H	4.98142000	0.95053500	-0.01789100

Table 2

Coordinate for optimized S1 of BTMC

C	-3.44150600	-0.24444200	0.00002100
C	-2.82551500	-1.48706100	0.00015200
C	-1.43405900	-1.43934300	0.00030100
C	-0.93061600	-0.11601800	0.00026000
S	-2.27308800	1.04019000	0.00014500
C	0.39496700	0.29851600	0.00018700
C	0.91133900	1.62685700	0.00014500
C	2.28698300	1.66825900	0.00001100
C	2.88349500	0.39141000	-0.00001900
S	1.70882100	-0.89428800	0.00007700
C	-4.90086400	0.04643300	-0.00062400
C	4.28200300	0.05432300	-0.00022900
O	4.70082800	-1.09758300	-0.00036400
H	-3.39879500	-2.40749000	0.00015300
H	-0.78405800	-2.30599400	0.00065000
H	0.26681000	2.49874900	0.00023100
H	2.87533500	2.57847200	-0.00004800
H	-5.47000500	-0.88618200	0.00260000
H	-5.19966300	0.63045400	0.87901400
H	-5.20000100	0.62442300	-0.88417200
H	4.97465400	0.92020900	-0.00028800

Table 3

Coordinate for optimized D0 of BTMC radical cation

C	-3.42791100	-0.23077500	-0.00975100
C	-2.82332700	-1.49386300	-0.00937300
C	-1.44450500	-1.43944800	-0.00408100
C	-0.93948700	-0.11863200	-0.00281500
S	-2.26072400	1.03219500	-0.00832100
C	0.40306200	0.28170700	-0.00156000
C	0.89653200	1.60513900	-0.00109400
C	2.28238700	1.66139500	0.00075500
C	2.86348000	0.39796200	0.00192100
S	1.71126500	-0.87665800	0.00075400
C	-4.88501900	0.06155100	0.01866400
C	4.30089600	0.05215900	0.00386000
O	4.66466000	-1.09910100	0.00466100
H	-3.40063800	-2.41050300	-0.01340000
H	-0.80225100	-2.31288700	-0.00302500
H	0.25304400	2.47758700	-0.00212200
H	2.86059600	2.57790000	0.00123900
H	-5.45346700	-0.80443000	-0.32595600
H	-5.20263600	0.28665700	1.04453900
H	-5.14152700	0.92450200	-0.60114900
H	5.00426900	0.90222500	0.00450500

Table 4

Coordinate for optimized D1 of BTMC radical cation

C	3.44375700	-0.20823100	0.00000300
C	2.87544600	-1.46739900	-0.00015900
C	1.47853000	-1.44279500	-0.00016100
C	0.95188400	-0.15470500	-0.00001400
S	2.24713200	1.02253000	0.00002200
C	-0.40076600	0.23084400	-0.00000300
C	-0.90637600	1.56234700	0.00008800
C	-2.26438200	1.62762000	0.00005700
C	-2.88994900	0.34387000	-0.00011700
S	-1.68361200	-0.93305500	-0.00010700
C	4.89801000	0.12795400	0.00041100
C	-4.23822800	0.13630300	-0.00019500
O	-4.85511000	-0.98230300	0.00003300
H	3.46741200	-2.37410600	-0.00026300
H	0.86546000	-2.33752100	-0.00025900
H	-0.25562700	2.42764400	0.00016700
H	-2.83398600	2.55032200	0.00011100
H	5.49218400	-0.78745600	-0.00264600
H	5.17013100	0.71649300	-0.88106100
H	5.17069900	0.71085400	0.88548200
H	-4.93925400	0.98573900	0.00010200

Table 5

Coordinate for optimized D0 of BTMC neutral radical

C	3.54538800	-0.21520800	-0.00045300
C	2.90367400	-1.48705000	0.00002300
C	1.52473700	-1.41925300	0.00012000
C	1.01415600	-0.11718700	0.00007800
S	2.31421100	1.05575000	0.00014400
C	-0.35615700	0.28721300	-0.00002300
C	-0.85864800	1.57947900	-0.00009600
C	-2.26363700	1.62142300	-0.00011300
C	-2.84121000	0.37356900	-0.00005400
S	-1.64729800	-0.88375500	-0.00009400
C	4.88184200	0.04605700	0.00010200
C	-4.25806600	0.05319000	-0.00001600
O	-4.70609500	-1.07527400	0.00019300
H	3.47269000	-2.40904700	-0.00013500
H	0.88119800	-2.29200600	0.00011000
H	-0.22612300	2.45919400	-0.00009000
H	-2.84469100	2.53709700	-0.00013400
H	5.59300100	-0.77224900	-0.00039900
H	5.27558900	1.05534300	0.00071600
H	-4.92597800	0.93854000	0.00016900

Table 6

Coordinate for optimized D1 of BTMC neutral radical

C	3.52567200	-0.22789300	0.00000900
C	2.90366600	-1.48606000	-0.00002100
C	1.50692900	-1.42444300	-0.00003500
C	1.00525400	-0.12818600	-0.00001100
S	2.30621600	1.03891700	-0.00001500
C	-0.35430800	0.28806100	-0.00000100
C	-0.86041700	1.60229500	-0.00001300
C	-2.23798400	1.66321500	0.00000700
C	-2.84686000	0.38425500	0.00003300
S	-1.65664500	-0.89307400	0.00000600
C	4.87964800	0.06739700	0.00002900
C	-4.23944900	0.06087400	0.00005500
O	-4.66480700	-1.09446600	-0.00001900
H	3.47414900	-2.40695600	-0.00002200
H	0.86440500	-2.29679800	-0.00005200
H	-0.21488300	2.47322900	-0.00002800
H	-2.81565200	2.57970400	0.00001100
H	5.60706300	-0.73572000	0.00005100
H	5.24657300	1.08613500	0.00003100
H	-4.92923900	0.92556200	-0.00001000

References:

1. Fujita, M.; Oguro, D.; Miyazawa, M.; Oka, H.; Yamaguchi, K.; Ogura, K., Self-assembly of ten molecules into nanometre-sized organic host frameworks. *Nature* **1995,** *378* (6556), 469-471.
2. Gera, R.; Das, A.; Jha, A.; Dasgupta, J., Light-induced proton-coupled electron transfer inside a nanocage. *Journal of the American Chemical Society* **2014,** *136* (45), 15909-15912.
3. Jha, A.; Chakraborty, D.; Srinivasan, V.; Dasgupta, J., Photoinduced charge transfer in solvated anthraquinones is facilitated by low-frequency ring deformations. *The Journal of Physical Chemistry B* **2013,** *117* (40), 12276-12285.
4. Neese, F., The ORCA program system. *Wiley Interdisciplinary Reviews: Computational Molecular Science* **2012,** *2* (1), 73-78.
5. Sure, R.; Grimme, S., Corrected small basis set Hartree-Fock method for large systems. *Journal of Computational Chemistry* **2013,** *34* (19), 1672-1685.
6. Becke, A. D., Density-functional exchange-energy approximation with correct asymptotic behavior. *Physical Review A* **1988,** *38* (6), 3098-3100.
7. Weigend, F.; Ahlrichs, R., Balanced basis sets of split valence, triple zeta valence and quadruple zeta valence quality for H to Rn: Design and assessment of accuracy. *Physical Chemistry Chemical Physics* **2005,** *7* (18), 3297-3305.
8. Kossmann, S.; Neese, F., Efficient Structure Optimization with Second-Order Many-Body Perturbation Theory: The RIJCOSX-MP2 Method. *Journal of Chemical Theory and Computation* **2010,** *6* (8), 2325-2338.
9. Weigend, F., Accurate Coulomb-fitting basis sets for H to Rn. *Physical Chemistry Chemical Physics* **2006,** *8* (9), 1057-1065.
10. Vosko, S. H.; Wilk, L.; Nusair, M., Accurate spin-dependent electron liquid correlation energies for local spin density calculations: a critical analysis. *Canadian Journal of Physics* **1980,** *58*, 1200-1211.
11. Hehre, W. J.; Stewart, R. F.; Pople, J. A., Self-Consistent Molecular-Orbital Methods. I. Use of Gaussian Expansions of Slater-Type Atomic Orbitals. *The Journal of Chemical Physics* **1969,** *51* (6), 2657-2664.
12. Hehre, W. J.; Ditchfield, R.; Pople, J. A., Self—Consistent Molecular Orbital Methods. XII. Further Extensions of Gaussian—Type Basis Sets for Use in Molecular Orbital Studies of Organic Molecules. *The Journal of Chemical Physics* **1972,** *56* (5), 2257-2261.